HHS Public Access

Author manuscript

Nat Photonics. Author manuscript; available in PMC 2012 December 01.

Published in final edited form as:

Nat Photonics. 2012 June 1; 6(6): 391–397. doi:10.1038/nphoton.2012.104.

Photovoltaic Retinal Prosthesis with High Pixel Density

Keith Mathieson[1,4,*], **James Loudin**[1,2,*,†], **Georges Goetz**[1,3], **Philip Huie**[1,2], **Lele Wang**[3], **Theodore I. Kamins**[3], **Ludwig Galambos**[3], **Richard Smith**[4], **James S. Harris**[3], **Alexander Sher**[4], and **Daniel Palanker**[1,2]

[1]Hansen Experimental Physics Laboratory, Stanford University

[2]Department of Ophthalmology, Stanford University

[3]Department of Electrical Engineering, Stanford University

[4]Santa Cruz Institute for Particle Physics, UC Santa Cruz

Abstract

Retinal degenerative diseases lead to blindness due to loss of the “image capturing” photoreceptors, while neurons in the “image processing” inner retinal layers are relatively well preserved. Electronic retinal prostheses seek to restore sight by electrically stimulating surviving neurons. Most implants are powered through inductive coils, requiring complex surgical methods to implant the coil-decoder-cable-array systems, which deliver energy to stimulating electrodes via intraocular cables. We present a photovoltaic subretinal prosthesis, in which silicon photodiodes in each pixel receive power and data directly through pulsed near-infrared illumination and electrically stimulate neurons. Stimulation was produced in normal and degenerate rat retinas, with pulse durations from 0.5 to 4 ms, and threshold peak irradiances from 0.2 to 10 mW/mm^2, two orders of magnitude below the ocular safety limit. Neural responses were elicited by illuminating a single 70 μm bipolar pixel, demonstrating the possibility of a fully-integrated photovoltaic retinal prosthesis with high pixel density.

Introduction

Retinal degenerative diseases such as Age Related Macular Degeneration (one of the leading causes of blindness in the developed world[1]) and Retinitis Pigmentosa (the leading cause of inherited blindness[2]) lead to loss of photoreceptors, while the inner retinal neurons survive to a large extent[3-5]. Electrical activation of these neurons can produce visual percepts

† Corresponding author.

*The first two authors contributed equally to the study, and share primary authorship.

Author Contributions: JL and DP jointly conceived and designed the pulsed-NIR photovoltaic retinal prosthesis system, and the three-diode pixel devices. KM, TK and JH led the fabrication team of LW and LG, with LW performing most of the fabrication steps that produced the implant device. AS and DP conceived the electrophysiology experiments that were carried out by KM, JL, GG, and RS under guidance of AS. KM and GG performed the data analysis with direction from AS. PH performed the subretinal implantations and histological analysis. JL wrote the first draft of the paper, with KM, AS, and DP contributing several sections and extensive edits. The project was organized and coordinated by DP.

(phosphenes), thereby providing an alternative route for visual information, raising hope for the restoration of sight to the blind.

Indeed, recent clinical trials with electrode arrays implanted either epiretinally (facing the ganglion cell side) or subretinally (facing the photoreceptor side) have restored visual acuity on the order of 20/1200 to subjects blinded by retinal degeneration[6,7]. While this serves as an important proof of concept with clinically useful implications, existing retinal prosthesis designs have a number of shortcomings.

Many implants deliver stimulation signals using serial telemetry and distribute them over the electrode array via an intraocular cable[6], a design that is difficult to scale to the large numbers of densely packed microelectrodes required for higher visual acuity. Additionally, the bulky intraocular receiving and processing electronics make surgery more complex and increase the probability of undesirable side effects[8]. Finally, retinal stimulation patterns in such systems are fully determined by images captured by the external camera, regardless of the eye orientation. Thus, patients cannot use natural eye movements to scan the visual scene – a very important feature of normal visual perception. Devices with photosensitive pixels (such as that from Retina Implant AG[7]) largely overcome the scalability limitation and make use of natural eye movements, but still depend on external power delivered via RF coils and a trans-scleral cable. Our design overcomes these problems by using micro-fabricated arrays of photodiodes driven photovoltaically. It has been shown that subretinal photovoltaic arrays can stimulate the retina in vivo and provide signals to the central visual system when illuminated by an intense full field near-infrared (NIR) flash[9]. However, until now all photosensitive electronic systems have been either too weak to produce patterned retinal stimulation[10], or have required a separate power source to amplify ambient optical signals[7].

Here we describe a photovoltaic retinal prosthesis system design in which video goggles deliver both power and visual information directly to each pixel through pulsed NIR illumination, eliminating the need for complex electronics and wiring schemes, and preserving the natural link between image perception and eye movement. We demonstrate the plausibility of this design through successful in-vitro stimulation of healthy and degenerate[11] rat retina with NIR light intensities at least two orders of magnitude below the ocular safety limit. We also demonstrate the possibility of high resolution stimulation with retinal responses elicited by a single 70 μm bipolar pixel containing a 20 μm active electrode and a local concentric return electrode for improved isolation from neighboring pixels.

Results

System Design

The photovoltaic retinal prosthetic system is shown in Figure 1. A pocket computer processes images captured by a miniature video camera. A near-to-eye projection system (similar to conventional video goggles) projects these images into the eye and onto a photodiode array using pulsed NIR (880-915 nm) light[12,13]. Photodiodes in each pixel of the subretinal array convert this light into pulsed photocurrent. Iridium oxide electrodes deliver these stimulating pulses to the retina, targeting primarily the surviving cells in the inner

nuclear layer (INL). While an epiretinal photovoltaic stimulation design is also feasible, subretinal stimulation of the graded-response inner retinal neurons may provide some advantages. For example, mediation by non-spiking neurons may result in a more natural conversion of the pulsed spatiotemporal stimulation pattern into bursts of spikes from the retinal ganglion cells (RGCs). This is in contrast to the exact pulse timing required for the direct activation of RGCs in the epiretinal approach.

Ambient light is too dim to produce sufficient photocurrent to directly stimulate neurons, by a factor of at least 1000[13,14]. Therefore, we employ a NIR laser image projection system that produces pulsed illumination of sufficient intensity to drive the photodiode array, while remaining invisible to any remaining photoreceptors. The pulsed light induces charge-balanced bi-phasic pulses in the silicon photodiode array, thereby avoiding electrode erosion and hydrolysis[15,16]. However, care must be taken to avoid excessive retinal heating. The light-induced temperature rise must be kept within the physiological range - below 1°C - as codified in ocular safety regulations[17]. Such thermal considerations limit average retinal irradiances to approximately 5.2mW/mm^2 at the 905nm wavelength used in this study[18] (see derivation in the Methods section). In addition to the cumulative effect of chronic exposure, the retina must not overheat during a single pulse. For pulse durations in the range of 0.05–70 ms, the limit for peak irradiance is given by the equation $285 \cdot t^{-0.25}$, where t is the pulse duration in ms and the result is in mW/mm^2 (see Methods section). For example, peak irradiance is limited to 285mW/mm^2 for a 1ms pulse at a 905nm wavelength.

Initial evaluation of our approach was performed using a photodiode array (ASR, Optobionics Corp.[19]) where each 25μm pixel contains a photodiode connected to a ~10 μm activated iridium oxide film electrode. Though all pixels share a single large return electrode located on the back of the ASR, each pixel independently converts locally-received light into cathodal-first, charge-balanced pulses (Figure 2a).

Achieving high spatial resolution may be complicated by the interference of currents from nearby pixels as they travel to the distant return electrode common to all pixels in this array design[12]. One way of reducing such cross-talk is to provide individual local return electrodes to each pixel. While this solves the problem of crosstalk, it also decreases the penetration depth of electric current into tissue[12]. For this reason and to increase the dynamic range of stimulation, our next generation devices have local return electrodes and 3 diodes per pixel, providing a substantially higher current density.

Triple-Diode Pixels

Single photodiode pixels produce up to 0.5V at physiologically safe light intensities[12,18]. Both *in vitro*[18] and *in vivo*[9] data indicate that this voltage can successfully stimulate the retina. However, larger voltages can be safely applied in a physiological environment[20-22]. Pixels with three diodes in series can produce 1.5V, which triples charge injection on the sputtered iridium oxide film electrodes, from 0.5mC/cm^2 for a single diode, to 1.5mC/cm^2 [18]. This increase requires 3 times higher light intensities, since the photosensitive pixel area is now divided into 3 sub-units. We have fabricated implants with 70 and 140μm pixels containing 20 and 40μm diameter stimulation electrodes; the corresponding pixel densities were 178 and 55 pixels/mm^2 (Figure 2b). All implants are

30μm thick, to provide sufficient depth for absorption of the NIR light in silicon (penetration depth of 905nm light in silicon is 35μm[23]), but thin enough to be implanted subretinally.

Two sizes of arrays have been constructed: 0.8×1.2mm for implantation into rats, and 2×2mm for implantation into larger animals. Trenches etched between neighboring pixels provide electrical isolation, eliminating pixel cross-talk within the silicon device. Each pixel has a local return electrode that constrains stimulation currents to nearby neurons, improving the achievable resolution of the prosthetic device.

Electrophysiological Testing

We tested the responses of six healthy and five degenerate[11] (RCS – Royal College of Surgeons) rat retinas to subretinal photovoltaic stimulation by recording RGC spikes induced by NIR stimuli. A schematic of the experimental setup is shown in Figure 3a. Briefly, we placed an isolated retina between the photodiode array and a multielectrode array (MEA) consisting of 512 electrodes spaced at 60μm[24], with the RGCs facing the recording electrodes. The photodiode array receives pulses of patterned NIR light projected through the transparent MEA and retina, and converts it to electrical currents. Spontaneous RGC spiking was recorded by the MEA and compared with RGC activity during the presentation of infrared and visible light (spatiotemporal white noise) stimulation, in the same preparation. The data underwent subtraction of the stimulation artifact and a neuron identification procedure[24-27] resulting in the detection of spike trains from individual RGCs. Supplementary Figure 1 outlines the data analysis in more detail.

The area of the MEA is 1.7mm^2, over which 100 individual neurons were typically detected. In the healthy wild-type rat retina, we observed reliable responses to NIR flashes of 0.5-4ms pulse width. Without the photodiode arrays, the retinal neurons did not respond to NIR light. The majority of neurons responded with the latencies of 10-70ms. Some neurons also exhibited responses with latencies in the 2-5ms range. Upon application of neurotransmitter blockers DNQX (70 μM) and L-AP7 (200μM) both groups of spikes disappeared, indicating that these responses were elicited by stimulation of the inner retina. Reliable identification of the sub-5ms spiking was challenging due to the strong stimulus artifact and therefore we excluded the sub-5ms latency responses from the subsequent quantitative analysis.

The single- and triple-diode devices elicited very similar responses. Figure 4 describes a representative peristimulus time histogram of a healthy retina's RGC response to NIR flashes of different peak irradiances and durations for the 140 μm triple-diode pixels. The change in the average number of elicited spikes with the duration and peak intensity of the NIR flashes (Figures 4c,d) shows that varying either parameter can modulate the retinal response. A strength-duration dependence of the stimulation threshold (defined as a 50% probability of eliciting a spike) is shown in Figures 5e,f, with standard deviation shown with hash marks. With the 140 μm 3-diode devices, the threshold for 1ms pulses was 0.9 ± 0.2mW/mm^2, decreasing to 0.3 ± 0.1 mW/mm^2 for 4ms pulses. For the single-diode devices, the stimulation threshold for wild-type retina was 0.8 ± 0.4mW/mm^2 with 1 ms pulses, decreasing to 0.2 ± 0.1mW/mm^2 with 4ms pulses (Supplemental Figure 2). These results were obtained using full-field illumination of the implants. All error bars in Figures 4 and 5a-d denote the standard error of the mean.

To check whether the observed RGC responses result from photoreceptor activation by the electric currents we selectively blocked synaptic transmission from photoreceptors to ON bipolar cells with L-AP4 (an mGluR6 receptor agonist, 100 μM). As expected, application of L-AP4 led to the disappearance of visible light responses in ON-center but not OFF-center RGCs, as assessed through the spike-triggered average of the RGC responses to the visible spatiotemporal white noise stimulus[24-27]. In contrast, the responses of the ON-center RGCs to electrical stimulation were unchanged, indicating that the stimulation is most likely not due to the photoreceptors themselves, but rather due to activation of the subsequent neuronal layers (see Supplementary Figure 3 for more details).

Degenerating retina is known to undergo significant anatomical restructuring[28,29]. We tested the effect of this degeneration on photovoltaic subretinal stimulation by performing similar experiments on RCS rat retinas 60 to 90 days postnatal, when the vast majority of photoreceptors have degenerated. We again were able to record from approximately 100 neurons in each preparation, with all five datasets showing clear stimulation with a similar spatial distribution to that observed in wild-type RGCs. Figure 5 shows a typical response of one of the RGCs to NIR flashes of various durations and intensities (data for a triple-diode device). Supplemental Figure 2 shows the corresponding data for the single-diode devices. Figure 5e,f shows the strength-duration dependences of the mean RGC stimulation thresholds for wild-type (N=15) and RCS (N=24) retinas activated by single-diode and triple-diode devices. The RCS retinal stimulation thresholds with triple-diode devices were approximately 2-3 times higher than in the wild-type; with single-diode devices this ratio increased up to 6. For example, the 1ms RCS stimulation threshold was 2mW/mm^2 with triple-diode devices, but 5mW/mm^2 with single-diode devices. At 4ms the thresholds decreased to 0.8mW/mm^2 for both the triple- and single-diode devices. The observed thresholds are about two orders of magnitude below ocular safety limits for both peak and average power (Figure 5e,f).

In all datasets retinal responses contained spike bursts where the number of spikes increased with both irradiance and pulse width, with a mean latency of ∼25ms in WT retinas and ∼35ms in RCS retinas. Bursts of spikes lasted approximately 40ms after the stimulus in WT retinas and 60ms in RCS retinas. For the single-diode monopolar devices, the maximum number of spikes in the burst saturated at the level of approximately 4 in WT retina and 3 in RCS. The triple diode devices were able to elicit bursts of up to 3 spikes in WT and RCS retinas for the irradiance values shown. However, bursts of up to 7 spikes could be elicited in both WT and RCS retinas with longer pulse durations and higher irradiance, illustrating the extended dynamic range of the triple-diode devices.

In wild-type retinas the firing rate increased from a spontaneous background of ∼3Hz to over 100Hz for a brief period (10-50ms) after the pulse. In the degenerate retina the spontaneous rate of RGC activity is known to be higher[30] and it increased from ∼15Hz to 85Hz within a time window of 10-65ms after the photovoltaic stimulation.

RGC activity was elicited from an RCS retina with NIR light spot size as small as 60×60μm with a threshold of 2.7mW/mm^2 using 4ms pulses on the single-diode device. Illuminating a single 140μm size triple-diode pixel elicited RCS retinal activity with a threshold of

4.1mW/mm^2 at a 4ms pulse duration. Similarly, illuminating a single 70μm triple-diode pixel for 4ms at 4.9mW/mm^2 elicited a threshold retinal response.

Discussion

Figures 3 and 4 demonstrate that elicited RGC responses can be modulated by both light intensity and pulse width. The described optical system uses a liquid crystal display (LCD) illuminated by a laser beam to form patterns of NIR light (see description in Methods section), enabling only intensity modulation within each video frame. However, since the retinal response can also be modulated by varying the pulse width, DLP™ technology based on an array of high-speed actuated micro-mirrors, can also be employed[31]. Such a device would allow both the duration and timing of exposure to be precisely controlled on the scale of individual pixels. In addition to higher throughput compared to an LCD, this high-speed control would allow the sequential activation of nearby pixels to further reduce pixel crosstalk.

The full-field stimulation thresholds were more than two orders of magnitude below ocular safety limit and were determined using cathodal-first stimulation pulses. Thresholds for single pixel stimulation were more than one order of magnitude below the ocular safety limits. This could perhaps be lowered, by up to 2-7 times, if anodal-first pulses are used[32]. Our fabrication process can be easily altered to accommodate the opposite polarity.

As stimulation thresholds rapidly increase with distance to the target cells[12,33], high resolution retinal stimulation requires close electrode-neuron proximity – apposition on the order of the size of the stimulating electrode[12]. To assess the proximity of the inner retinal neurons to subretinal implants we fabricated 30 μm-thick (matching our active devices) polymer (Microchem SU8) implants that can be sectioned together with tissue for histology. These devices were coated with SIROF to match our electrode material and implanted in the subretinal space of RCS rats for 6 weeks[34]. The histological section of an RCS rat retina shown in Figure 6a demonstrates that the inner nuclear layer (INL) is separated from the implant surface by 5 – 25μm. Electric current must penetrate at least this depth to ensure effective neural stimulation.

We have computed the current density distribution from single pixels of various dimensions with the COMSOL Conductive Media DC package, where the retina is modeled as a resistive medium. Figure 6a presents the current density in front of a 115μm pixel with a 40 μm active electrode and circumferential returns, superimposed upon a histological section of a flat implant in the subretinal space of an RCS rat. The current penetrates sufficiently deep to provide targeted stimulation of many neurons in the INL. However, smaller, 62μm pixels with 20μm active electrodes can affect fewer such neurons, and will likely require either increased light intensity or improved proximity for effective stimulation.

We have previously shown that retinal cells migrate inside and around three-dimensional sub-retinal implants, an effect that may be utilized to attain intimate neuron-electrode proximity[35]. The histological section shown in Figure 6b depicts an array of 15μm diameter, 65μm tall pillars six weeks after implantation. The bipolar cells surround the pillar tops,

placing them in cellular-scale proximity to the tips of the pillar electrodes. The computed current distribution for this geometry overlays the histological section, demonstrating that such pillar arrays can effectively deliver stimulation currents to the inner nuclear layer, and could provide a mechanism for reducing the thresholds and improving stimulation localization in future devices.

Finally, the need to conform to eye curvature inherently limits the sizes of rigid implants to at most a few millimeters. The use of a flexible silicon substrate[36] can overcome this limitation and allow larger arrays to deform elastically to the curvature of the eye. Trenches etched between neighboring pixels leave 0.5 μm thin silicon "springs" (Supplemental Figure 4a,b). Optical coherence tomography shows a 6 mm-wide sample array with 75μm pixels conforming to the curvature of a pig retina (Supplemental Figure 4c) despite its very large size, a feat made possible by the inherent 2-dimensional deformability of the flexible silicon mesh.

Since the photovoltaic implant is thin and wireless, the surgical procedure is much simpler than in other retinal prosthetic approaches. As in conventional subretinal surgery, the procedure involves a partial vitrectomy followed by a subretinal injection to create a retinal bleb. The implant is then inserted into the subretinal space through a retinal incision, and the retina is reattached[19]. As large incisions can complicate retinal re-attachment, retinotomies should be as small as practically possible. Since all pixels in the implant function independently several smaller arrays may be inserted through the same retinotomy to tile a large area.

In conclusion, we demonstrate that NIR light-induced photovoltaic stimulation using a subretinal photodiode array elicits bursts of RGC spikes in both healthy and degenerate rat retinas at irradiances substantially below ocular safety limits. The response can be modulated by either pulse duration or irradiance in each pixel. Such a fully integrated wireless implant promises the restoration of useful vision to patients blinded by degenerative retinal diseases.

Methods

Infrared projection system

As LEDs cannot meet the brightness requirement of our implant[12], the infrared projection system employs an array of laser diodes coupled into a multimode fiber to produce high-intensity illumination with reduced coherence. A microlens array diffuser improves homogeneity and introduces a 5 degree angular spread to the collimated beam. Speckling at the image plane has been measured to be less than 1% (standard deviation). An ocular lens images a transmissive LCD panel onto the retina, similar to conventional video goggles but with ∼1000 times greater peak brightness[12].

Triple-diode pixels

The triple-diode pixel photovoltaic arrays shown in Figure 5 were manufactured on silicon-on-insulator wafers using a six mask lithographic process. Light absorbed in the silicon is converted into charge-balanced bi-phasic pulse of electric current flowing through the tissue

between the active and return electrodes[18]. A detailed discussion of the fabrication technique is to be published elsewhere.

Multielectrode Array Recordings

Electrophysiological experiments began with enucleation of the eye from an anesthetized (35 mg/kg ketamine, 5 mg/kg xylazine, 0.01 mg/kg glycopyrrolate) rat, which was subsequently euthanized. A small piece of retina (~ 3 mm × 3 mm) was isolated and placed between the recording array (ganglion cell side) and the photodiode array (photoreceptors side), as shown in Figure 2. The retina was perfused with Ames' solution bubbled with 95% oxygen and 5% carbon and kept at 25 to 30 °C. At least 400 NIR pulses were applied for each parameter setting at repetition rate of 2 Hz. Recorded voltage waveforms from each of the 512 electrodes were analyzed with the spike-finding software described previously[24-27]. We calculated stimulation threshold as the irradiance required for 50% spike initiation efficiency, i.e. eliciting on average one spike for every two stimuli. Experiments were performed on 5 healthy wild-type rats and 4 RCS rats, which model retinal degeneration[11]. All experimental procedures were conducted in accordance with institutional guidelines and conformed to the guidelines of the Association for Research in Vision and Ophthalmology (ARVO) Statement for the Use of Animals in Ophthalmic and Vision Research.

Optical Safety Considerations

NIR light (880-905 nm) is absorbed primarily by pigmented tissues such as the retinal pigment epithelium, with a practically negligible absorption coefficient (<0.06 cm^{-1}) in transparent ocular layers such as the cornea, lens, and neural retina. According to ocular safety standards[37,38], the maximum permissible radiant power ($MP\Phi$) which may be chronically delivered to the retina is $MP\Phi = 6.93\times10^{-5}C_TC_EP^{-1}$, where $C_T=10^{0.002(\lambda-700)}$ in the 700-1050 nm range, with $C_T=2.5$ at λ=905 nm. C_E depends on the angular spread of the incident beam and for retinal spot sizes greater than 1.7 mm in diameter is 29.3 W/mm^2. P is the pupil factor which models pupil constriction or dilation, and is exactly 1 for infrared wavelengths in the absence of dilating drugs. For the 905 nm wavelength used in this study the average irradiance limit is 5.2 mW/mm^2. For single-pulse exposure, the peak-irradiance limit in the 0.05 – 70 ms duration range is described by the equation[30,31] $MP\Phi = 6.93*10^{-4}C_TC_Et^{-0.25}$, where t is in seconds. At 905 nm, $MP\Phi = 285\cdot t^{-0.25}$, where t is in ms and the result is in mW/mm^2. Both the chronic limit and the single pulse limit are plotted in Figure 4e as a function of pulse duration, assuming a pulse repetition rate of 15 Hz.

Temperature rise during in-vitro stimulation

Light incident on a photovoltaic prosthesis produces heat, resulting in a small temperature rise in the retina. NIR light has a penetration depth in silicon on the order of 30 μm[23], the temperature rise by the end of a 1 ms pulse at an irradiance of 1 mW/mm^2 does not exceed 0.002 °C (for a 30 μm thick device in water). With a repetition rate of 2 Hz, corresponding to duty cycle of 0.2%, the average temperature rise of a device during prolonged irradiation in a perfused chamber is even lower. Such a minute temperature rise cannot elicit neural stimulation, nor damage tissue.

Supplementary Material

Refer to Web version on PubMed Central for supplementary material.

Acknowledgments

The authors thank Optobionics Inc. and especially George McLean for providing the ASR samples, and Peter Peumans and Rostam Dinyari from the Electrical Engineering Department at Stanford University for providing a sample of the flexible silicon grid[36] for tests of its flexibility in a porcine eye. We also thank A.M. Litke, S. Kachiguine, A. Grillo and W. Dabrowski for the development of the 512-electrode recording system, and M. Krause for his help with retinal preparations. The authors thank M.F. Marmor, M.S. Blumenkranz, R. Gariano, and S. Sanislo from the Department of Ophthalmology at Stanford for productive discussions of the implant design and surgical procedures. We thank Stuart Cogan at EIC Labs for fabrication advice and for iridium oxide electrode deposition, Maureen McCall at the University of Louisville for a critical manuscript reading, and Machelle Pardue at Emory University for advice on subretinal implantations into RCS rats.

Funding was provided by the National Institute of Health Grant R01-EY-018608, by Air Force Office of Scientific Research grant FA9550-04, Stanford Bio-X IIP grant. KM was supported through an SU2P fellowship as part of an RCUK Science Bridges award. JL was supported in part by the NSF Graduate Research Fellowship program. AS was supported in part by Burroughs Welcome Fund Career Award at the Scientific Interface.

References

1. Smith W, et al. Risk factors for age-related macular degeneration: Pooled findings from three continents. Ophthalmology. 2001; 108:697–704. [PubMed: 11297486]
2. Haim M. Epidemiology of retinitis pigmentosa in Denmark. Acta Ophthalmol Scand Suppl. 2002:1–34. [PubMed: 11921605]
3. Kim SY, et al. Morphometric analysis of the macula in eyes with disciform age-related macular degeneration. Retina. 2002; 22:471–477. [PubMed: 12172115]
4. Mazzoni F, Novelli E, Strettoi E. Retinal ganglion cells survive and maintain normal dendritic morphology in a mouse model of inherited photoreceptor degeneration. J Neurosci. 2008; 28:14282–14292. 28/52/14282 [pii] 10.1523/JNEUROSCI.4968-08.2008. [PubMed: 19109509]
5. Stone JL, Barlow WE, Humayun MS, de Juan E Jr, Milam AH. Morphometric analysis of macular photoreceptors and ganglion cells in retinas with retinitis pigmentosa. Arch Ophthalmol. 1992; 110:1634–1639. [PubMed: 1444925]
6. Ahuja AK, et al. Blind subjects implanted with the Argus II retinal prosthesis are able to improve performance in a spatial-motor task. Br J Ophthalmol. 2010; 95:539–543. bjo.2010.179622 [pii] 10.1136/bjo.2010.179622. [PubMed: 20881025]
7. Zrenner E, et al. Subretinal electronic chips allow blind patients to read letters and combine them to words. Proc R Soc B. 2010; 278:1489–1497. rspb.2010.1747 [pii] 10.1098/rspb.2010.1747.
8. Besch D, et al. Extraocular surgery for implantation of an active subretinal visual prosthesis with external connections: feasibility and outcome in seven patients. British Journal of Ophthalmology. 2008; 92:1361–1368. [PubMed: 18662916]
9. DeMarco P, et al. Stimulation via a Subretinally Placed Prosthetic Elicits Central Activity and Induces a Trophic Effect on Visual Responses. Investigative Ophthalmology & Visual Science. 2007; 48:916–926. [PubMed: 17251495]
10. Pardue M, et al. Possible sources of neuroprotection following subretinal silicon chip implantation in RCS rats. Journal of Neural Engineering. 2005; 2:S39–S47. [PubMed: 15876653]
11. Bourne MC, Campbell DA, Tansley K. Hereditary Degeneration of the Rat Retina. Br J Ophthalmol. 1938; 22:613–623. [PubMed: 18169569]
12. Loudin JD, et al. Optoelectronic retinal prosthesis: system design and performance. Journal of Neural Engineering. 2007; 4:S72–S84. 10.1088/1741-2560/4/1/S09. [PubMed: 17325419]
13. Palanker DV, et al. Design of a high-resolution optoelectronic retinal prosthesis. Journal of Neural Engineering. 2005; 2:S105–S120. [PubMed: 15876646]
14. Stelzle M, Stett A, Brunner B, Graf M, Nisch W. Electrical Properties of Micro-Photodiode Arrays for Use as Artificial Retina Implant. Biomedical Microdevices. 2001; 3:133–142.

15. Brummer SB, Turner MJ. Electrical-Stimulation of Nervous-System - Principle of Safe Charge Injection with Noble-Metal Electrodes. Bioelectrochemistry and Bioenergetics. 1975; 2:13–25.
16. Cogan SF, Guzelian AA, Agnew WF, Yuen TG, McCreery DB. Over-pulsing degrades activated iridium oxide films used for intracortical neural stimulation. Journal of Neuroscience Methods. 2004; 137:141–150. [PubMed: 15262054]
17. in *Directive 90/385/EEC* (2004).
18. Loudin J, Cogan S, Mathieson K, Sher A, Palanker D. Photodiode Circuits for Retinal Prostheses. IEEE Trans Biomed Circ and Syst. 2011; 5:468–480.
19. Chow A, et al. The Artificial Silicon Retina Microchip for the Treatment of Vision Loss From Retinitis Pigmentosa. Arch Ophthalmol. 2004; 122:460–469. [PubMed: 15078662]
20. Beebe X, Rose T. Charge injection limits of activated iridium oxide electrodes with 0.2 ms pulses in bicarbonate buffered saline (neurological stimulation application). IEEE Transactions on Biomedical Engineering. 1988; 35:494–495. [PubMed: 3397105]
21. Cogan S, Troyk P, Ehrlich J, Plante T, Detlefsen D. Potential-Biased, Asymmetric Waveforms for Charge-Injection with Activated Iridium Oxide (AIROF) Neural Stimulation Electrodes. IEEE Trans Biomed Eng. 2006; 53:327–332. [PubMed: 16485762]
22. Negi S, Bhandari R, Rieth L, Van Wagenen R, Solzbacher F. Neural electrode degradation from continuous electrical stimulation: Comparison of sputtered and activated iridium oxide. Journal of Neuroscience Methods. 2010; 186:8–17. 10.1016/j.jneumeth.2009.10.016. [PubMed: 19878693]
23. Green MA, Keevers MJ. Optical-Properties of Intrinsic Silicon at 300 K. Prog Photovoltaics. 1995; 3:189–192.
24. Litke AM, et al. What does the eye tell the brain?: Development of a system for the large-scale recording of retinal output activity. Ieee T Nucl Sci. 2004; 51:1434–1440. 10.1109/Tns.2004.832706.
25. Field GD, et al. High-sensitivity rod photoreceptor input to the blue-yellow color opponent pathway in macaque retina. Nat Neurosci. 2009; 12:1159–1164. nn.2353 [pii] 10.1038/nn.2353. [PubMed: 19668201]
26. Field GD, et al. Spatial properties and functional organization of small bistratified ganglion cells in primate retina. J Neurosci. 2007; 27:13261–13272. 27/48/13261 [pii] 10.1523/JNEUROSCI.3437-07.2007. [PubMed: 18045920]
27. Petrusca D, et al. Identification and characterization of a Y-like primate retinal ganglion cell type. J Neurosci. 2007; 27:11019–11027. 27/41/11019 [pii] 10.1523/JNEUROSCI.2836-07.2007. [PubMed: 17928443]
28. Jones BW, Marc RE. Retinal remodeling during retinal degeneration. Exp Eye Res. 2005; 81:123–137. [PubMed: 15916760]
29. Jones BW, et al. Retinal remodeling triggered by photoreceptor degenerations. J Comp Neurol. 2003; 464:1–16. [PubMed: 12866125]
30. Pu M, Xu L, Zhang H. Visual Response Properties of Retinal Ganglion Cells in the Royal College of Surgeons Dystrophic Rat. Investigative Ophthalmology & Visual Science. 2006; 47:3579–3585. [PubMed: 16877432]
31. Putman PH. Projector light engines - Digital light processing: A most magical mirror. Entertain Des. 2000; 34:11–11.
32. Jensen RJ, Rizzo JF. Thresholds for activation of rabbit retinal ganglion cells with a subretinal electrode. Experimental Eye Research. 2006; 83:367–373. 10.1016/j.exer.2006.01.012. [PubMed: 16616739]
33. Sekirnjak C, et al. High-resolution electrical stimulation of primate retina for epiretinal implant design. Journal of Neuroscience. 2008; 28:4446–4456. [PubMed: 18434523]
34. Butterwick A, et al. Effect of shape and coating of a subretinal prosthesis on its integration with the retina. Exp Eye Res. 2009; 88:22–29. [PubMed: 18955050]
35. Palanker D, et al. Migration of retinal cells through a perforated membrane: implications for a high-resolution prosthesis. Invest Ophthalmol Vis Sci. 2004; 45:3266–3270. [PubMed: 15326150]
36. Dinyari R, Rim SB, Huang K, Catrysse PB, Peumans P. Curving monolithic silicon for nonplanar focal plane array applications. Applied Physics Letters. 2008; 92:091114.

37. ANSI. Vol. ANSI 136.1-2000 (The Laser Institute of America, 2000).
38. DeLori F, Webb R, Sliney D. Maximum permissable exposures for ocular safety (ANSI 2000), with emphasis on ophthalmic devices. Journal of the Optical Society of America A. 2007; 24:1250–1265.

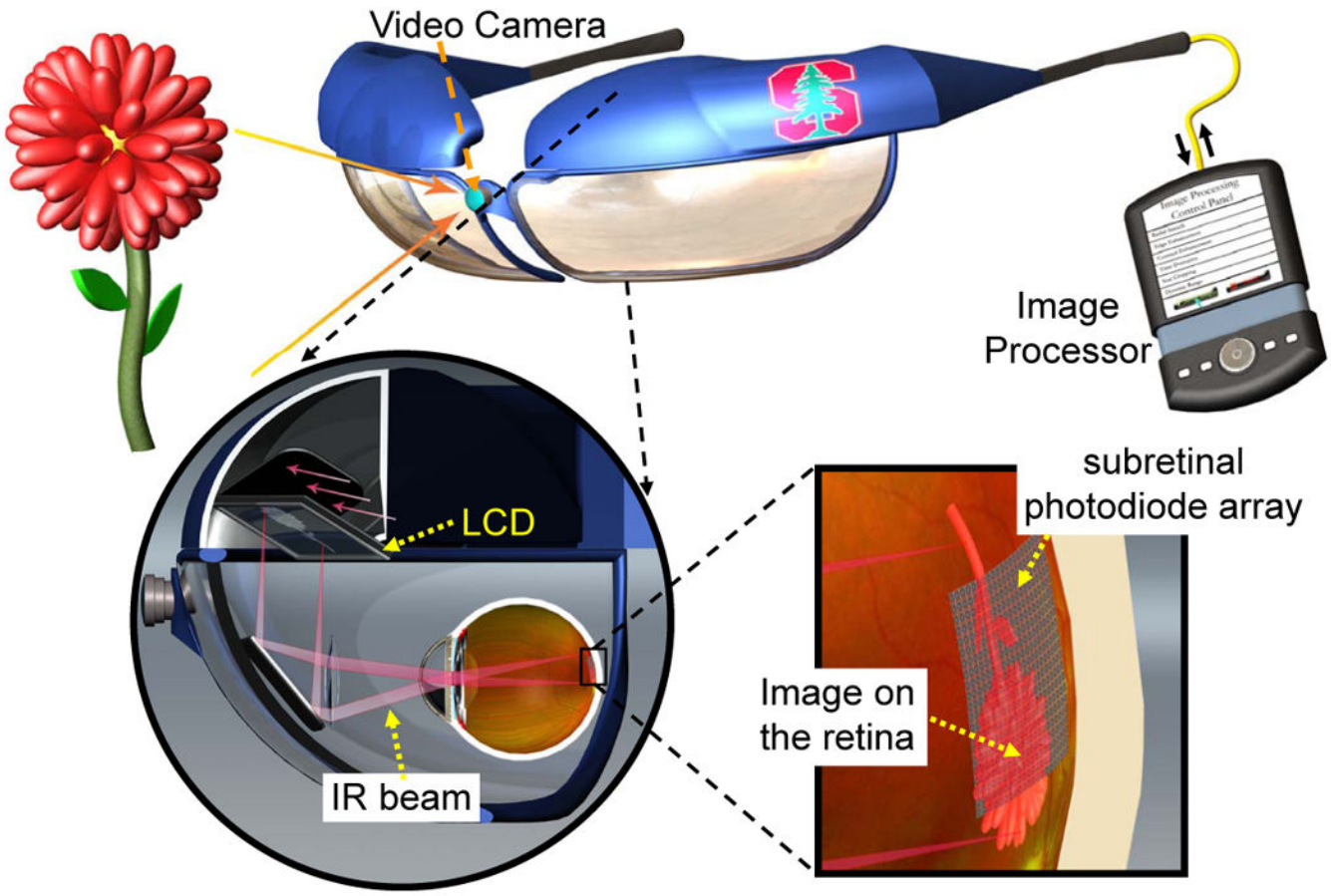

Figure 1.

Simplified system diagram. A portable computer processes video images captured by a head-mounted camera. Video goggles then project these images onto the retina using pulsed infrared (880-915 nm) illumination. Finally, pixels in the subretinal photodiode array convert this light into local stimulation currents.

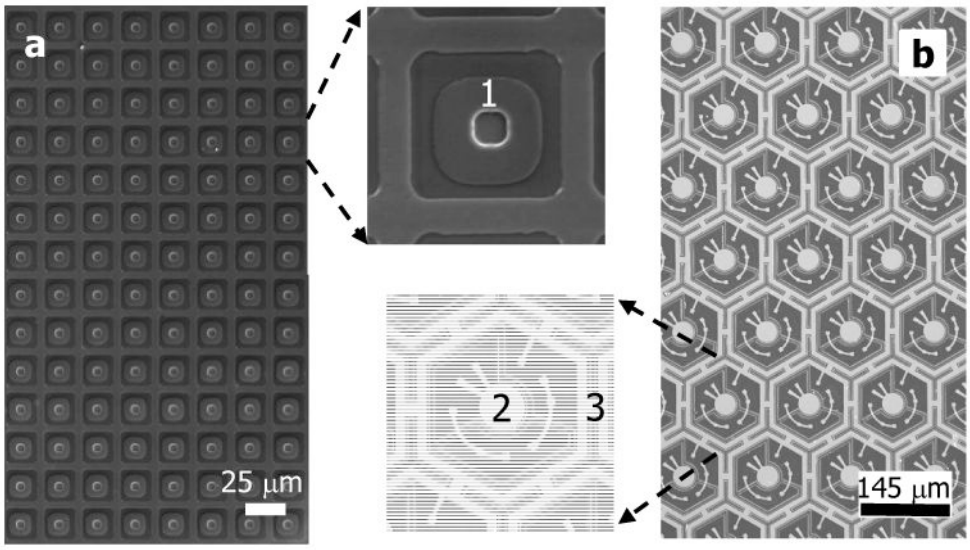

Figure 2.

(a) A photodiode array consisting of 25μm pixels, each containing a ∼10 μm stimulating electrode (#1 in inset) surrounded by the photosensitive area of a single photodiode. Return electrode common to all pixels is situated on the back of the array.

(b) An array with 3-diode pixels arranged in a hexagonal pattern. Pixels of 70 and 140 μm in size have been made. Central electrodes (#2 in inset) of 20 and 40 μm in diameter, respectively, are surrounded by 3 diodes connected in series, and by the common return electrode (#3 in inset). Pixels are separated by 5μm trenches to improve perfusion and for better isolation. 140 μm pixel is shown in the inset.

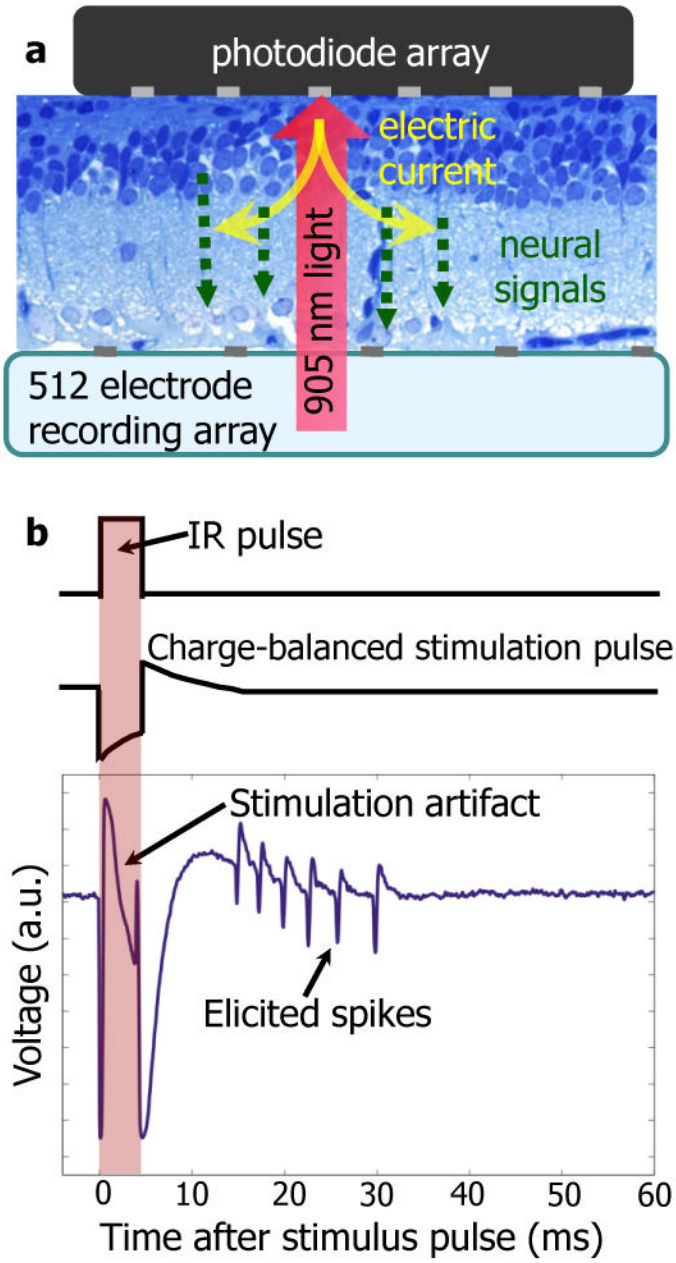

Figure 3.

(a) Schematic of photovoltaic stimulation characterization system. Both healthy and degenerate rat retinas were placed between the stimulating and recording arrays, with the ganglion cell layer facing the recording electrodes. The photodiode array converts patterned 880-905 nm illumination into stimulation currents.

(b) An IR pulse, with variable pulse width and intensity, creates a charge-balanced current waveform in each pixel of the photodiode array. The microelectrode array records the resultant stimulus artifact and retinal responses from each of the 512 electrodes. Stimulation is repeated at least 400 times for each setting. The artifact is then subtracted and the

recorded action potentials undergo principal component analysis and automated clustering to attribute spiking waveforms to over 100 RGCs per experiment.

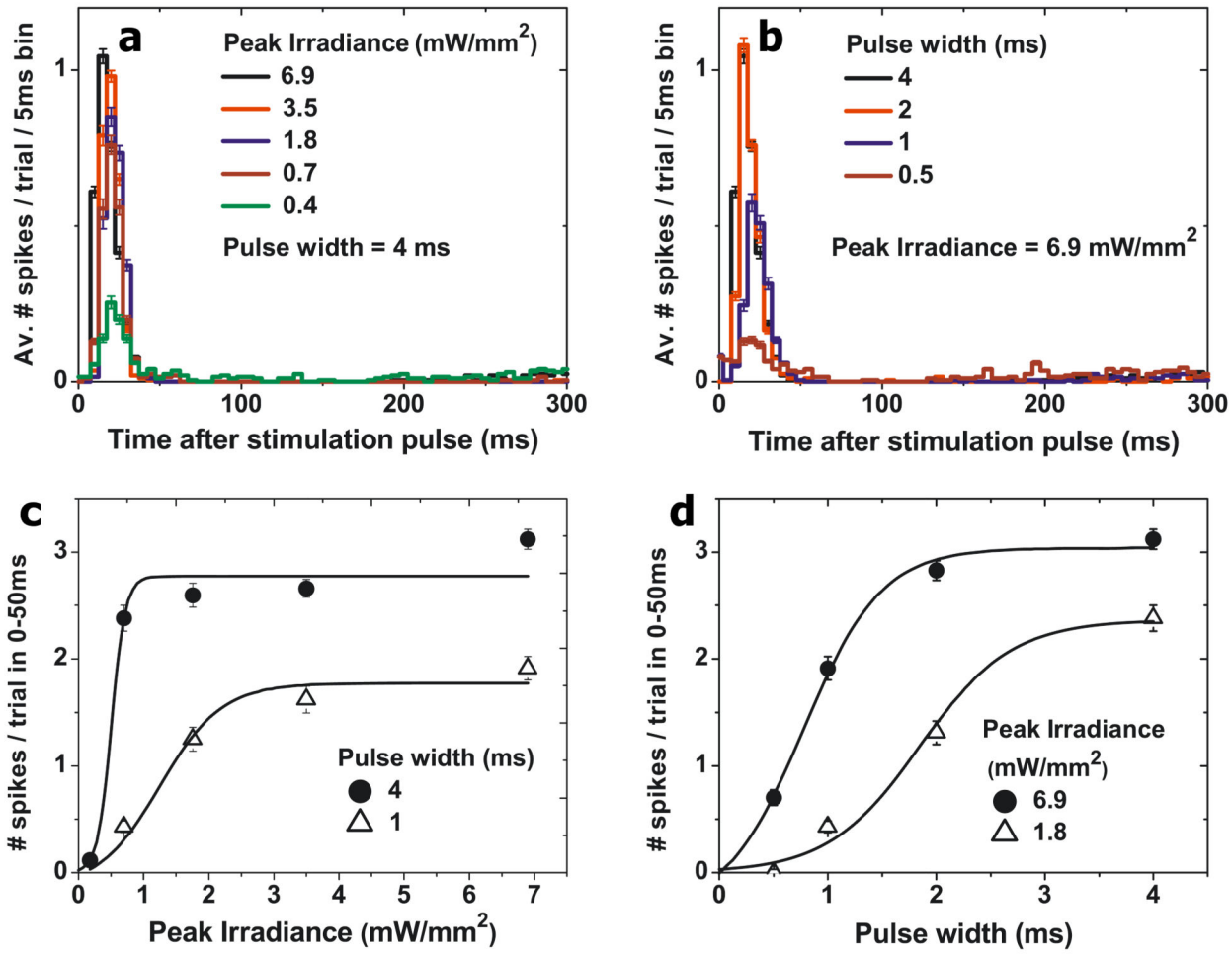

Figure 4.

(a) Peristimulus time histograms showing the stimulated response of a wild type rat retina, using the triple-diode devices, to different peak irradiances at a fixed pulse width of 4ms. (b) Peristimulus time histograms for various pulse widths at a fixed irradiance of 6.9 mW/mm^2. (c) Increase of retinal response with peak irradiance for two pulse widths. (d) Increase of retinal response with pulse width for two peak irradiances. All error bars denote the standard error of the mean.

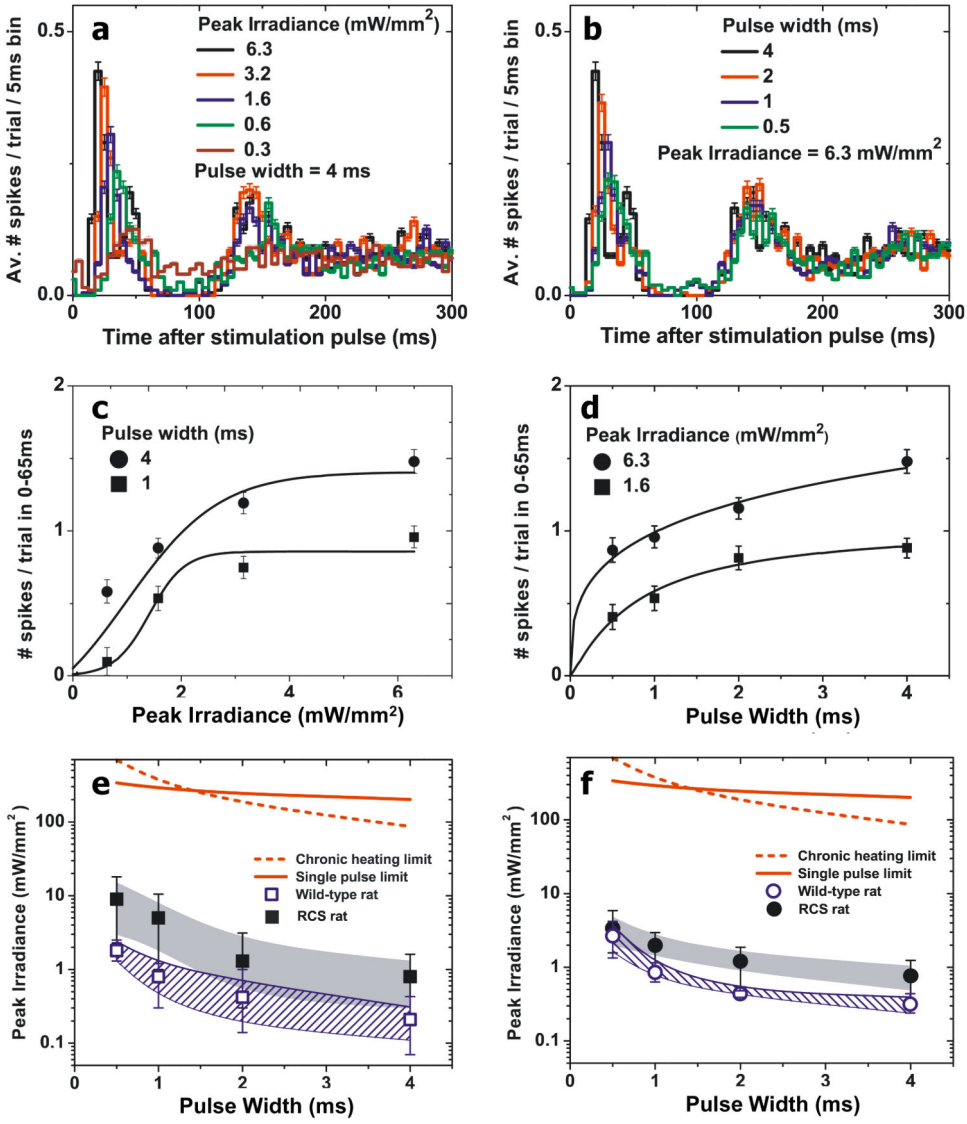

Figure 5.

(a) Peristimulus time histograms showing the elicited response of RCS rat retina, using the triple-diode devices, at a fixed NIR pulse width and (b) at a fixed light intensity. The number of elicited spikes increases with irradiance (c) and with pulse width (d). (e) Strength-duration plot for both wild type and RCS rat retinas, showing the average stimulation thresholds for 10 neurons in both the healthy and degenerate retinas (single-diode devices). The average values for the triple-diode devices are also plotted for 6 neurons over two preparations (WT) and 14 neurons in a single preparation (RCS).Hashed zones depict the range of standard deviation, while the whiskers show min and max for each data point. The optical safety limits for a single pulse and continuous retinal illumination (15 Hz repetition rate) with 905 nm light are also plotted. The error bars in parts a-d denote the standard error of the mean.

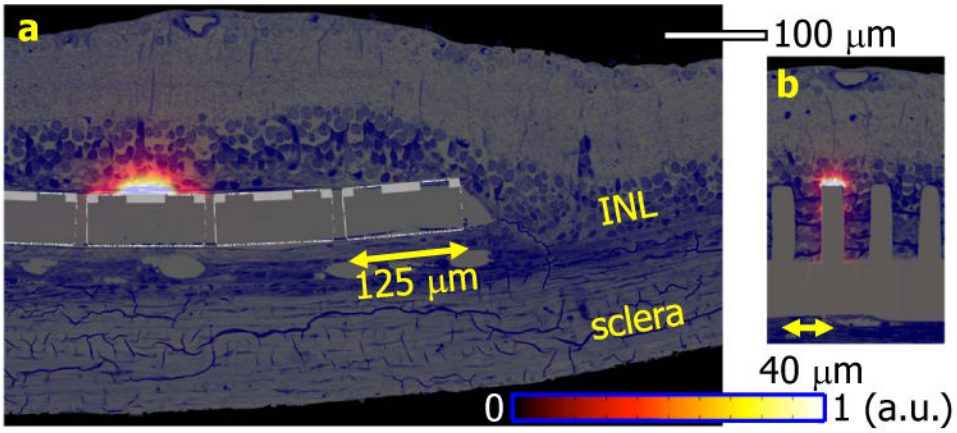

Figure 6.

(a) Retinal histology of a flat polymer implant in the subretinal space of an RCS rat, with the numerically calculated current distribution from a 115 μm pixel (pixel schematics overlaid). (b) Retinal histology of a pillar array implant, overlaid with the numerically calculated current distribution from electrodes placed on the tops. Implants with pixel densities greater than 256 pixels/mm^2 will likely require the use of such 3-D geometries to achieve sufficient proximity to target neurons.